

## Membrane-Bound Dimer Structure of a $\beta$ -Hairpin Antimicrobial Peptide from Rotational-Echo Double-Resonance Solid-State NMR<sup>†</sup>

R. Mani,<sup>‡</sup> M. Tang,<sup>‡</sup> X. Wu,<sup>‡</sup> J. J. Buffy,<sup>‡,§</sup> A. J. Waring,<sup>||</sup> M. A. Sherman,<sup>⊥</sup> and M. Hong<sup>\*,‡</sup>

*Department of Chemistry, Iowa State University, Ames, Iowa 50011, Department of Medicine, University of California at Los Angeles School of Medicine, Los Angeles, California 90095, and Department of Biomedical Informatics, City of Hope National Medical Center, Duarte, California 91010*

*Received February 13, 2006; Revised Manuscript Received May 12, 2006*

**ABSTRACT:** The intermolecular packing of a  $\beta$ -hairpin antimicrobial peptide, PG-1, in lipid bilayers is determined using solid-state NMR distance measurements. Previous spin counting experiments showed that PG-1 associates as dimers in POPC bilayers; however, the detailed dimer structure was unknown. We have now measured several intermolecular  $^{13}\text{C}$ – $^{19}\text{F}$ ,  $^1\text{H}$ – $^{13}\text{C}$ , and  $^{15}\text{N}$ – $^{13}\text{C}$  distances in site-specifically labeled PG-1 to constrain the structure of the intermolecular interface. The distances are measured using the rotational-echo double-resonance (REDOR) technique under magic-angle spinning. The results indicate that two PG-1 molecules align in a parallel fashion with the C-terminal strand of the hairpin forming the dimer interface. Six hydrogen bonds stabilize this interface, and the Phe<sub>12</sub> side chain adopts the  $g^-$  conformation in the membrane as in solution. The parallel packing of the peptide in the lipid bilayer differs from the antiparallel dimer found in DPC micelles and may be stabilized by its strong amphipathic character, which should facilitate its insertion into the amphipathic lipid bilayer. This study demonstrates the utility of the REDOR NMR technique for the elucidation of the oligomeric structure of membrane proteins.

A large number of small cationic peptides produced by animals and plants kill bacterial, fungal, and viral cells by destroying their cell membranes (1, 2). Various mechanisms have been proposed to explain this membrane disruption. In the barrel-stave model, several peptides form transmembrane pores that deplete the membrane potential. In the carpet model, the peptides aggregate on the surface of the lipid bilayer, cause membrane thinning, and at high concentrations micellize the membrane. In the toroidal pore model, the peptides induce torus-shaped pores, where the two lipid leaflets bend toward each other and merge (3–5). One common feature of these mechanistic models is that the peptides oligomerize in order to disrupt the membrane integrity. However, direct determination of the oligomeric structure of antimicrobial peptides in lipid bilayers is so far scarce (6). Protegrin-1 (PG-1)<sup>1</sup> is a disulfide-linked  $\beta$ -hairpin antimicrobial peptide found in porcine leukocytes (7). Its Arg-rich sequence,  $\beta$ -hairpin conformation, and broad-spectrum activities are representative of many other antimicrobial peptides (8). To elucidate the mechanism of action

of PG-1, knowledge of the three-dimensional oligomeric structure of the peptide in the lipid bilayer is crucial.

Using a new  $^{19}\text{F}$  exchange NMR technique, we recently showed that the  $\beta$ -turn region of PG-1 is dimerized in POPC bilayers (9). In this experiment, dipolar-driven magnetization exchange among molecules of different orientations changes the  $^{19}\text{F}$  chemical shift frequency, which in turn reduces the intensity of a spin echo. For an oligomeric species with  $M$  orientationally inequivalent molecules, the equilibrium echo intensity is  $1/M$ . Thus, measurement of the echo intensity at long mixing times allows the determination of the oligomeric number. The strong  $^{19}\text{F}$ – $^{19}\text{F}$  dipolar coupling allows the detection of spins as far as  $\sim 15$  Å away. In this way, we found that 4- $^{19}\text{F}$ -Phe<sub>12</sub> at the  $\beta$ -turn of PG-1 is dimerized within a  $\sim 15$  Å radius (9).

The next question to address is the structure of the PG-1 dimer. What is the mutual orientation of the two  $\beta$ -hairpins? Which of the two strands in each  $\beta$ -hairpin forms the dimer interface? What is the hydrogen-bonding pattern at the dimer interface? How does the PG-1 oligomeric structure facilitate its membrane disruptive function? Finally, how is the oligomeric structure dictated by the amino acid sequence, in terms of properties such as the distribution of polar and nonpolar residues? Addressing these questions is important not only for understanding the specific antimicrobial mechanism of PG-1 but also for obtaining general insights into the folding of  $\beta$ -sheet membrane proteins (10, 11).

In this work, we employ rotational-echo double-resonance (REDOR) NMR, a technique that measures heteronuclear distances (12), to determine the dimer structure of PG-1 in POPC bilayers. Using  $^{13}\text{C}$ – $^{19}\text{F}$ ,  $^1\text{H}$ – $^{13}\text{C}$ , and  $^{15}\text{N}$ – $^{13}\text{C}$

<sup>†</sup> This work is supported by National Institutes of Health Grants GM-066976 to M.H. and AI-37945 to A.J.W.

\* Corresponding author. Tel: 515-294-3521. Fax: 515-294-0105. E-mail: mhong@iastate.edu.

<sup>‡</sup> Iowa State University.

<sup>§</sup> Present address: Department of Chemistry and Biochemistry, University of Minnesota, Minneapolis, MN 55455.

<sup>||</sup> University of California at Los Angeles School of Medicine.

<sup>⊥</sup> City of Hope National Medical Center.

<sup>1</sup> Abbreviations: PG-1, protegrin-1; REDOR, rotational-echo double resonance; POPC, 1-palmitoyl-2-oleoyl-*sn*-glycero-3-phosphatidylcholine.

distance measurements on site-specifically labeled PG-1, we determined which strand forms the dimer interface, the mutual orientation of the  $\beta$ -hairpins, and the registry of hydrogen bonds at the dimer interface.

## MATERIALS AND METHODS

1-Palmitoyl-2-oleoyl-*sn*-glycero-3-phosphatidylcholine (POPC) was purchased from Avanti Polar Lipids (Alabaster, AL). PG-1 was synthesized according to previously published procedures (13). Two peptide samples were prepared: a 1:1 molar mixture of [ $^{15}\text{N}$ -Cys $_{15}$ ]PG-1 and [ $^{13}\text{C}'$ -Cys $_{15}$ ]PG-1, and [4- $^{19}\text{F}$ -Phe $_{12}$ ,  $^{13}\text{C}'$ -Val $_{16}$ ]PG-1. Synthesized PG-1 contains residual trifluoroacetate (TFA) ions, whose  $^{19}\text{F}$  spins can interfere with the  $^{13}\text{C}$ – $^{19}\text{F}$  distance measurement. We removed this residual TFA by repeated washing of the peptide in dilute HCl solutions until negligible signal was detected at  $-75$  ppm in the  $^{19}\text{F}$  solution NMR spectrum. The purified peptide was codissolved with POPC lipids in methanol and chloroform solutions to achieve the desired peptide/lipid (P/L) molar ratio. A P/L of 1:20 was used for the  $^{15}\text{N}$  and  $^{13}\text{C}'$  mixed labeled sample, and a P/L of 1:12.5 was used for the  $^{19}\text{F}$ ,  $^{13}\text{C}'$  doubly labeled sample. The combined solution was dried under a stream of nitrogen gas and lyophilized. The dry powder was packed into 4 mm rotors and hydrated to 35% water by mass. This hydration level was the same as that used previously for observing lipid  $^{31}\text{P}$  spectra in the presence of PG-1 (13). A glass spacer was used to center the sample in the rotor to reduce radio-frequency field inhomogeneity.

**Solid-State NMR.** NMR experiments were performed on a Bruker Avance DSX-400 spectrometer (Karlsruhe, Germany) operating at 400.49 MHz for  $^1\text{H}$ , 376.8 MHz for  $^{19}\text{F}$ , 100.72 MHz for  $^{13}\text{C}$ , and 40.58 MHz for  $^{15}\text{N}$ . The  $^{13}\text{C}\{^{19}\text{F}\}$  REDOR experiments, where the nucleus in the brackets is the unobserved dephasing spin, was conducted on a 4 mm magic-angle spinning (MAS) probe equipped with a Bruker HFX unit, which allows simultaneous tuning of  $^1\text{H}$  and  $^{19}\text{F}$  on the  $^1\text{H}$  channel. The  $^1\text{H}\{^{13}\text{C}\}$  and  $^{15}\text{N}\{^{13}\text{C}\}$  REDOR experiments were carried out on a  $^1\text{H}/^{13}\text{C}/^{15}\text{N}$  triple-resonance MAS probe. Spinning speeds were regulated to  $\pm 3$  Hz using a pneumatic control unit. To suppress lipid and peptide motion, which reduces dipolar couplings, all REDOR experiments were performed at 233 K, using air cooled through a Kinetic Thermal Systems XR air-jet sample cooler (Stone Ridge, NY). The  $^{31}\text{P}$  spectra of the lipids are fully reproducible before and after sample freezing, indicating that the peptide–lipid interaction is unaffected by freezing and thawing.  $^{13}\text{C}$  and  $^{15}\text{N}$  chemical shifts were referenced externally to the  $^{13}\text{C}'$  signal of  $\alpha$ -Gly at 176.4 ppm on the TMS scale and the  $^{15}\text{N}$  signal of *N*-acetylvaline at 122 ppm, respectively.

**$^{13}\text{C}\{^{19}\text{F}\}$  and  $^{15}\text{N}\{^{13}\text{C}\}$  REDOR Experiments.** The pulse sequence for the  $^{13}\text{C}\{^{19}\text{F}\}$  and  $^{15}\text{N}\{^{13}\text{C}\}$  REDOR experiments is shown in Figure 1a. The X-magnetization evolves under the X{Y} dipolar coupling, which is recoupled under MAS by a train of  $\pi$  pulses spaced half a rotor period apart (12). All except for one  $\pi$  pulse were applied on the Y channel. The single X  $\pi$  pulse was placed in the middle of the REDOR mixing period to refocus the X isotropic chemical shift. Two experiments were conducted for each mixing time: a control experiment ( $S_0$ ) where all of the Y-spin pulses

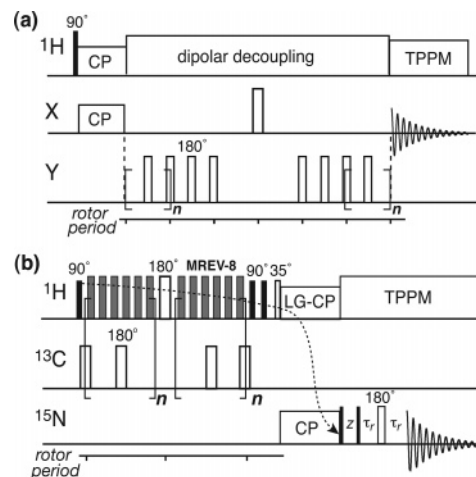


FIGURE 1: Pulse sequence for measuring intermolecular distances in site-specifically labeled PG-1. (a) X{Y} REDOR, where the X-spin is observed and the Y-spin pulses reduce the X-spin echo via the dipolar coupling. The  $^{13}\text{C}\{^{19}\text{F}\}$  and  $^{15}\text{N}\{^{13}\text{C}\}$  REDOR experiments were conducted using this sequence. (b)  $^{15}\text{N}$ -Detected  $^1\text{H}\{^{13}\text{C}\}$  REDOR. Filled and open rectangles indicate  $90^\circ$  and  $180^\circ$  pulses, respectively. TPPM: two-pulse phase modulation (40). LG-CP: Lee–Goldburg cross polarization (41). For both experiments, the  $180^\circ$  dephasing pulses were implemented as the composite pulse  $90^\circ 180^\circ 90^\circ$  to compensate for pulse length imperfections (14).

are turned off and a dephasing experiment ( $S$ ) where the Y pulses are on. The normalized dephasing,  $S/S_0$ , as a function of mixing time gives the dipolar coupling of interest without  $T_2$  relaxation effects.

To compensate for pulse imperfections, composite  $90^\circ_{\phi-90} 180^\circ_{\phi} 90^\circ_{\phi-90}$  pulses were used for the Y-spin pulses (14). The phase  $\phi$  was cycled according to the XY-8 scheme (15). This composite-pulse REDOR experiment was demonstrated to improve the accuracy of the distance measurements by compensating for pulse angle errors (14). Typical  $\pi$  pulse lengths were 10  $\mu\text{s}$  for  $^{13}\text{C}$  and  $^{15}\text{N}$  and 11  $\mu\text{s}$  for  $^{19}\text{F}$ .  $^1\text{H}$  decoupling field strengths were typically 60–70 kHz during acquisition and increased to 75–85 kHz during the REDOR mixing times to minimize the problem of incomplete REDOR dephasing (14). The spinning speed was 6 kHz for  $^{13}\text{C}\{^{19}\text{F}\}$  REDOR and 3.472 kHz for  $^{15}\text{N}\{^{13}\text{C}\}$  REDOR.

The error bars of  $S/S_0$ ,  $\epsilon_{S/S_0}$ , were propagated from the signal-to-noise ratios (SNR) of the  $S_0$  and  $S$  spectra, using the equation  $\epsilon_{S/S_0} = (S/S_0)(\epsilon_S^2 + \epsilon_{S_0}^2)^{1/2}$ , where the uncertainty  $\epsilon$  of each spectrum is  $1/\text{SNR}$ .

**$^{15}\text{N}$ -Detected  $^1\text{H}\{^{13}\text{C}\}$  REDOR Experiment.** Figure 1b shows the pulse sequence for the  $^{15}\text{N}$ -detected  $^1\text{H}\{^{13}\text{C}\}$  REDOR experiment (16, 17).  $^1\text{H}$  magnetization evolves under the recoupled  $^1\text{H}$ – $^{13}\text{C}$  dipolar interaction while the  $^1\text{H}$ – $^1\text{H}$  dipolar coupling is suppressed by an MREV-8 pulse train (18, 19). Two  $\pi$  pulses are applied on the  $^{13}\text{C}$  channel in each rotor period while a single  $^1\text{H}$   $\pi$  pulse is applied in the center of the C–H REDOR period to refocus the  $^1\text{H}$  isotropic chemical shift. At the end of the C–H REDOR period, a 75  $\mu\text{s}$  Lee–Goldburg cross-polarization (LG-CP) step is applied to selectively transfer the C–H dipolar modulated  $^1\text{H}$  magnetization to its directly bonded  $^{15}\text{N}$  nucleus for detection.

To optimize the MREV-8 performance and minimize the number of REDOR  $\pi$  pulses, the  $^1\text{H}\{^{13}\text{C}\}$  REDOR experiment was conducted at a slow spinning speed of 3.472 kHz. The MREV-8 pulse length was 3.5  $\mu\text{s}$  and was optimized

by maximizing the  $^{15}\text{N}$  intensity in the absence of the  $^{13}\text{C}$   $\pi$  pulses. The  $\pi$  pulse lengths were 9.8  $\mu\text{s}$  for  $^{13}\text{C}$  and 6.0  $\mu\text{s}$  for  $^1\text{H}$ . The  $^{13}\text{C}$  carrier frequency was placed on-resonance with the carbonyl signal to minimize off-resonance effects.

**REDOR Simulations and Molecular Modeling.** Two-spin REDOR curves were simulated using an in-house Fortran program. Three-spin REDOR curves for the C'–F experiment were simulated using the SIMPSON program (20). The simulations assumed  $\delta$ -function pulses and used the REPULSION scheme (21) for powder averaging. Input distances and angles for the REDOR simulations were obtained from model building in the Insight II environment (Accelrys, San Diego, CA), using minimum energy solution NMR structures of PG-1 as the monomer structure (PDB code 1PG1) (22). Since each pair of labels gives two distances at the dimer interface, the calculated REDOR curve for each pair of labels is the average of two couplings. For the equimolar mixture of  $^{13}\text{C}'$ -Cys<sub>15</sub> PG-1 and  $^{15}\text{N}$ -Cys<sub>15</sub> PG-1, the calculated REDOR curves were scaled by 50% to account for the fact that only 50% of the  $^{15}\text{N}$ -labeled peptide is directly adjacent to a  $^{13}\text{C}$ -labeled peptide. An additional scaling factor  $k$  due to incomplete dimerization was also taken into account in the REDOR simulations, by using  $(S/S_0) = k(S/S_0)_{\text{calc},100\%} + (1 - k)$ .

PG-1 dimer models that are potentially consistent with all of the experimentally measured distances were created using MODELLER (23) (version 6.1). In addition to the REDOR-based distance restraints, the input file included a restraint to preserve the intramolecular hydrogen bond ladder of each monomer and a restraint to maintain monomer symmetry. A representative low-energy conformer that agrees with all of the intermolecular distance constraints, the hydrogen bond registry, and the Phe<sub>12</sub>  $\chi_1$  angle has been deposited in the PDB with the code 1ZY6.

## RESULTS

**PG-1 Dimer Models.** Our previous  $^{19}\text{F}$  spin diffusion experiment of PG-1 in POPC bilayers established that the  $\beta$ -turn of the peptide, where 4- $^{19}\text{F}$ -Phe<sub>12</sub> is located, is dimerized (9). To determine the detailed dimer structure, we first consider the possible packing and alignment motifs for two  $\beta$ -hairpin molecules.

A  $\beta$ -hairpin peptide can form six distinct dimer motifs stabilized by intermolecular hydrogen bonds. The dimer interface could consist of two C-terminal strands from two monomers (NCCN), two N-terminal strands (CNNC), or one N-strand and one C-strand (NCNC). For each packing motif, the strands can align in a parallel or antiparallel fashion. In all six motifs, the molecules are packed sideways in the  $\beta$ -hairpin plane as constrained by the direction of the C=O $\cdots$ H–N hydrogen bonds. Figure 2 illustrates these six dimer models, with intermolecular hydrogen bond lengths,  $R_{\text{N–O}}$ , of 2.5–3.5 Å (24). These are satisfied for most interfacial residues except for the N- and C-terminal residues due to their larger disorder in the solution structure (22). For the distance measurements reported here, all labeled sites are located in the central region of the C-strand; thus the distances are minimally affected by dynamic disorder even if any persists in the lipid bilayer.

The dimer models of Figure 2 can be distinguished from each other by various intermolecular distances. For example,

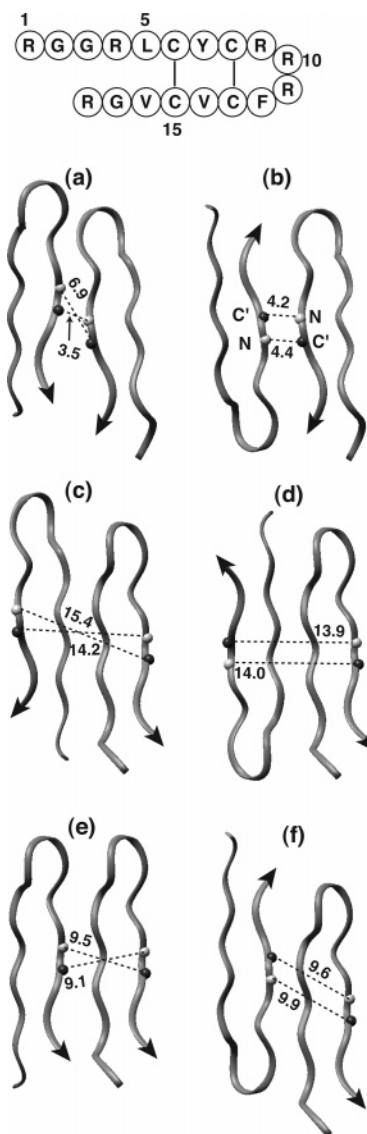


FIGURE 2: (a, b) NCCN, (c, d) CNNC, and (e, f) NCNC packing motifs of PG-1, whose amino acid sequence is shown at the top. The relative orientation of the  $\beta$ -hairpins is parallel in (a), (c), and (e) and antiparallel in (b), (d), and (f). Distances (in Å) between Cys<sub>15</sub>  $^{13}\text{C}'$  (filled circle) and Cys<sub>15</sub>  $^{15}\text{N}$  (open circle) are indicated as an example of the drastically different intermolecular distances among these packing motifs.

the intermolecular Cys<sub>15</sub>  $^{13}\text{C}'$ –Cys<sub>15</sub>  $^{15}\text{N}$  distances are less than 7 Å in the two NCCN models (a and b) but are 14–16 Å in the CNNC models (c and d) and 9–10 Å in the NCNC (e and f) packing models. Thus, the measurement of the Cys<sub>15</sub>–Cys<sub>15</sub>  $^{15}\text{N}\{^{13}\text{C}'\}$  distance, for example, can determine the strand identities at the dimer interface.

Figure 3 shows the  $^{15}\text{N}\{^{13}\text{C}'\}$  REDOR spectra of the equimolar mixture of [ $^{13}\text{C}'$ -Cys<sub>15</sub>]PG-1 and [ $^{15}\text{N}$ -Cys<sub>15</sub>]PG-1 in POPC bilayers at P/L = 1:20. The spectra were acquired with a REDOR mixing time of 13.8 ms, and a  $S/S_0$  value of 0.85 was measured. Since each PG-1 molecule contains only one isotopic label, the measured distance is purely intermolecular in origin. To account for dephasing by the natural abundance  $^{13}\text{C}$  background, a control experiment was carried out using only [ $^{15}\text{N}$ -Cys<sub>15</sub>]PG-1, which gave a  $S/S_0$  value of 0.94 at the same mixing time. Since  $(S/S_0)_{\text{labeled}} = 1 + (S/S_0)_{\text{total}} - (S/S_0)_{\text{unlabeled}}$ , the net dephasing by Cys<sub>15</sub>  $^{13}\text{C}'$  is  $0.91 \pm 0.05$ . This is significant compared to the calculated

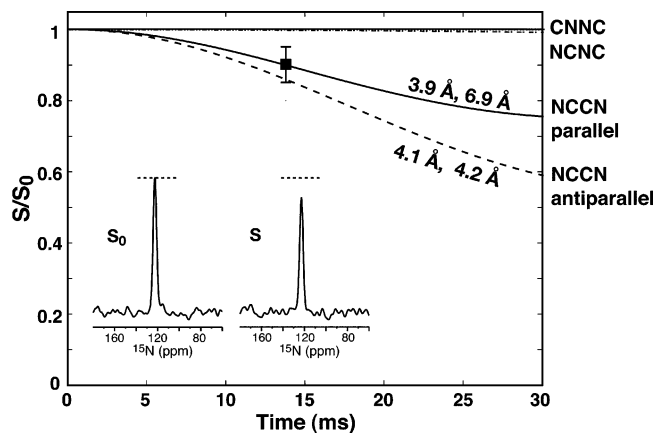


FIGURE 3: Experimental  $^{15}\text{N}\{^{13}\text{C}\}$  REDOR data of the 1:1 mixture of  $[^{13}\text{C}'\text{-Cys}_{15}]$ PG-1 and  $[^{15}\text{N-Cys}_{15}]$ PG-1 in POPC bilayers (P/L = 1:20). The  $S_0$  and  $S$  spectra at 13.8 ms are shown. The natural-abundance corrected  $S/S_0$  value is  $0.91 \pm 0.05$ . Among the calculated REDOR curves for various dimer models, the CNNC and NCNC models have no intensity decays in 30 ms while the NCCN models give measurable REDOR decays due to the much shorter distances. A scaling factor of 88% for incomplete dimerization was used for the calculated REDOR intensities.

REDOR dephasing for the CNNC and NCNC models. As shown in Figure 3, these packing models give C–N distances of 9 Å or longer, which produce no detectable  $^{15}\text{N}\{^{13}\text{C}\}$  REDOR dephasing in 30 ms. In contrast, the two NCCN models, which place the two labels within 4–7 Å, give sizable  $S/S_0$  values of 0.85–0.90 by 15 ms. These calculated REDOR curves took into account a dimer fraction of 88%, obtained from the C–H REDOR data below and from the previous CODEX experiments (9). Therefore, the  $^{15}\text{N}\{^{13}\text{C}\}$  REDOR data, while insufficient to give quantitative distances, qualitatively and unambiguously rule out the NCNC and CNNC packing motifs. Similarly, the sizable  $^1\text{H}\{^{13}\text{C}\}$  and  $^{13}\text{C}\{^{19}\text{F}\}$  REDOR decays found below, between labels placed on the C-strand of the peptide, conclusively rule out the NCNC or CNNC packing models. Moreover, the  $^{13}\text{C}\{^{19}\text{F}\}$  and  $^1\text{H}\{^{13}\text{C}\}$  REDOR data give quantitative distances that define the mutual orientation of the  $\beta$ -hairpin at the C-strand interface.

$^{13}\text{C}\{^{19}\text{F}\}$  REDOR. Since  $^{15}\text{N}$ – $^{13}\text{C}$  dipolar couplings are weak for distance above 4 Å, and Cys<sub>15</sub> is centrally located on the C-strand, the  $^{15}\text{N}\{^{13}\text{C}\}$  REDOR experiment is relatively insensitive to the mutual orientation of the two strands at the dimer interface. To extract the orientation information, we measured the C'–F distance on  $[4\text{-}^{19}\text{F-Phe}_{12}, ^{13}\text{C}'\text{-Val}_{16}]$ PG-1 in POPC bilayers. The two labels are spaced far apart on the C-strand; thus the distance between them is sensitive to the relative orientation of the two  $\beta$ -hairpins. The high  $\gamma$  of the  $^{19}\text{F}$  spin increases the dipolar coupling strength so that longer distances can be measured. Figure 4 shows the  $^{13}\text{C}$ -detected  $^{19}\text{F}$ -dephased REDOR data and a representative pair of spectra (a). The dephasing of the natural abundance carbonyl signals of the lipids and PG-1 by the  $^{19}\text{F}$  label was corrected from the data using the equation

$$\left(\frac{S}{S_0}\right)_{\text{labeled}} = \left[\left(\frac{S}{S_0}\right)_{\text{total}} - (1-f)\left(\frac{S}{S_0}\right)_{\text{unlabeled}}\right] \frac{1}{f} \quad (1)$$

where  $f$  is the fraction of the  $S_0$  signal due to the labeled

$^{13}\text{C}$ . Spectral comparison of the  $^{13}\text{C}$ -labeled and unlabeled samples gave an  $f$  of 80%. The dephasing of the natural abundance  $^{13}\text{C}'$  signal was directly measured through a control experiment on  $[4\text{-}^{19}\text{F-Phe}_{12}]$ PG-1 without any  $^{13}\text{C}$  labels. The  $S/S_0$  values were  $\sim 0.95$ . From these, we obtained the REDOR dephasing values of the labeled Val<sub>16</sub>  $^{13}\text{C}'$ , which are plotted in Figure 4b–d.

To fit the  $^{13}\text{C}$ – $^{19}\text{F}$  REDOR data, we consider both the intramolecular and intermolecular couplings, since each peptide contains both the  $^{13}\text{C}'$  and  $^{19}\text{F}$  labels. The average intramolecular Val<sub>16</sub> C'–Phe<sub>12</sub> F distance of the 20 minimum energy PG-1 solution structures is 11.8 Å with a standard deviation of  $\pm 0.8$  Å. The REDOR curve for this intramolecular distance alone (dotted line in Figure 4b) clearly decays more slowly than the experimental data, thus verifying the presence of additional intermolecular dipolar couplings. To obtain a model-independent intermolecular distance, we fit the data using a simple three-spin model where one C'–F distance is fixed at 11.8 Å while the other is varied. The angle between the two vectors is set at  $75^\circ$ , which is a typical value obtained from model building of PG-1 and which does not affect the REDOR curves significantly within  $\pm 20^\circ$ . The calculated  $^{13}\text{C}\{^{19}\text{F}\}$  REDOR curves used a dimer fraction of 88%, determined from CODEX experiments on POPC-bound PG-1 at the same P/L ratio (9). The model-independent three-spin simulations are shown in Figure 4b: the experimental data fall within an intermolecular distance range of 9.5–12 Å, with the best fit at 11 Å.

We next consider the intermolecular Val<sub>16</sub>–Phe<sub>12</sub> C'–F distances in parallel and antiparallel NCCN dimers (Figure 5). The parallel packing gives much longer distances than the antiparallel packing. Each dimer contains two intermolecular distances: in parallel dimers, one distance is short ( $\sim 10$  Å) and the other is long ( $\sim 16$  Å), while in antiparallel dimers the two distances are similar and both short (5–8 Å). Thus the parallel alignment should give slower dipolar dephasing than the antiparallel dimer structure. Since the model-independent best-fit result of 11 Å falls into the parallel-packed intermolecular distance regime (Figure 4b), which does not overlap with the short intermolecular distances of the antiparallel dimer, we conclude that the PG-1  $\beta$ -hairpins must adopt the parallel NCCN dimer structure.

Figure 4c shows model-dependent simulations of REDOR curves based on the distance geometries in Figure 5. Since the dimer interface has two intermolecular distances, each calculated REDOR curve is the average of two three-spin geometries, where each three-spin network contains the fixed intramolecular distance (11.8 Å) and an intermolecular distance. The parallel NCCN dimer simulations are indicated as a shaded area to reflect the distance variations due to the monomer structure distribution (22). The shorter intermolecular distance in the parallel dimer models ranges from 8.4 to 11 Å, while the longer distance ranges from 15.3 to 16.5 Å. The data fall within this parallel dimer range. The best fit to the experimental data is found at intermolecular distances of 9.3 and 15.7 Å (solid line in Figure 4c). In comparison, the REDOR curves for the antiparallel NCCN dimer structures (dashed lines) decay to much lower intensities than the experimental data and thus can be ruled out.

The position of the fluorine atom on the Phe<sub>12</sub> aromatic ring depends on the  $\chi_1$  torsion angle. The solution structure of PG-1 shows a well-defined Phe<sub>12</sub> side chain with a  $\chi_1$

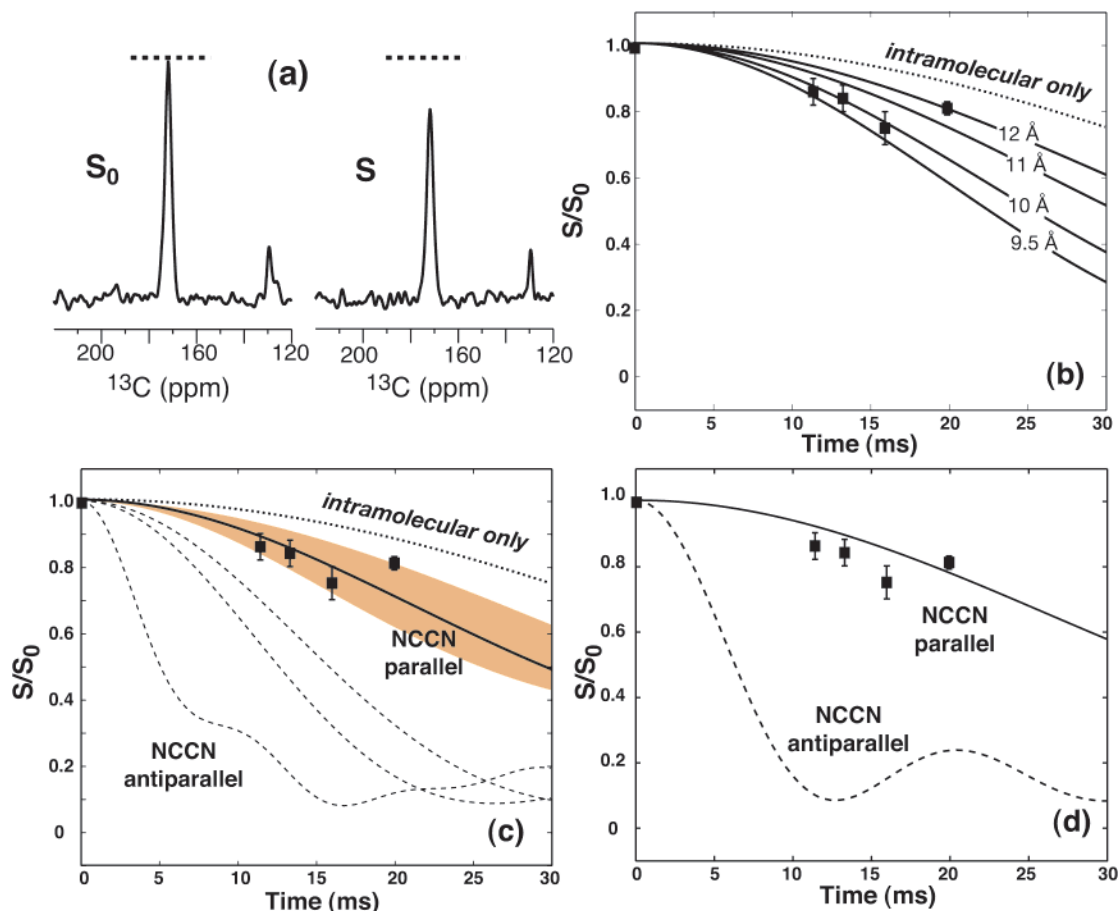


FIGURE 4: Experimental  $^{13}\text{C}\{^{19}\text{F}\}$  REDOR data of  $[4\text{-}^{19}\text{F}\text{-Phe}_{12}, ^{13}\text{C}'\text{-Val}_{16}]$ PG-1 in POPC bilayers (P/L = 1:12.5) and calculated REDOR curves for various structural models. (a) Representative  $S_0$  and  $S$  spectra, acquired at a mixing time of 16 ms. (b) Experimental  $S/S_0$  values after natural abundance correction (squares). These are much lower than the calculated REDOR curve for the intramolecular  $\text{C}'\text{-F}$  distance of 11.8 Å alone (dotted line), indicating that additional intermolecular couplings are present. Solid lines: model-independent three-spin REDOR curves for an intermolecular distance between 9.5 and 12 Å and an intramolecular distance of 11.8 Å. The calculated REDOR curves used a dimer fraction of 88%. (c) Model-dependent REDOR curves. NCCN parallel dimers: shaded area. The experimental data fall within this range and are best fit with intermolecular distances of 9.3 and 15.7 Å (solid line). NCCN antiparallel dimers: dashed lines, with intermolecular distances of 4.9–8.5 Å. These are completely outside the experimental data and can be ruled out. (d) Calculated  $\text{C}'\text{-F}$  REDOR curves for parallel (solid line) and antiparallel (dashed line) NCCN dimers of a nearly ideal  $\beta$ -strand.

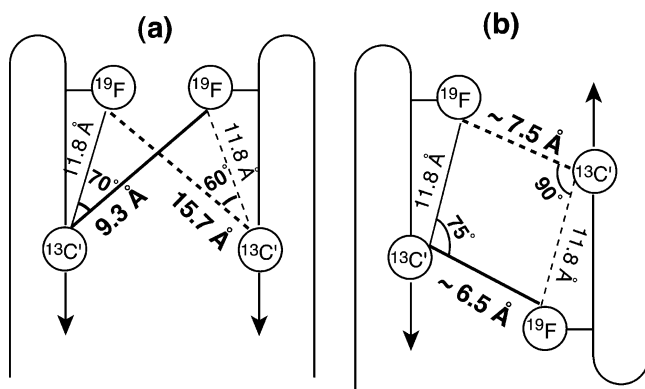


FIGURE 5: Schematic representation of the intermolecular and intramolecular  $\text{Val}_{16}^{13}\text{C}'\text{-Phe}_{12}^{19}\text{F}$  distances and the angle between them in (a) the NCCN parallel dimer and (b) the NCCN antiparallel dimer.

angle of  $70 \pm 3.5^\circ$  (22). This corresponds to the second most populated rotameric state ( $g^-$ ) of Phe in  $\beta$ -sheets (25). This  $\chi_1$  angle places the phenylene ring close to its own backbone. The PG-1 dimer models indicate that  $\chi_1 = 180^\circ$  (trans) and  $\chi_1 = -60^\circ$  ( $g^+$ ) result in side chain–backbone steric conflict

between the two monomers. Even when the  $\phi$ ,  $\psi$  angles of turn residues are modified to avoid this steric conflict, the intermolecular  $\text{C}'\text{-F}$  distances for the trans (7 and 14 Å) and  $g^+$  conformers (15 and 21 Å) clearly disagree with the experimental data. Thus, Phe<sub>12</sub> adopts the same  $g^-$  conformation in the lipid bilayer as in solution.

The PG-1 solution structure used in dimer model building does not have perfect  $\beta$ -strand torsion angles. Thus the question arises as to whether the parallel NCCN dimer conclusion would hold if the peptide adopts a more ideal  $\beta$ -strand structure in the lipid bilayer. To address this question, we constructed an ideal  $\beta$ -strand with  $\phi$ ,  $\psi$  angles of  $-140^\circ$ ,  $140^\circ$  to represent the C-strand of PG-1 from Phe<sub>12</sub> to Arg<sub>18</sub>. Parallel and antiparallel dimers of this ideal  $\beta$ -strand were built using standard hydrogen bond lengths. The resulting intermolecular  $\text{Val}_{16}^{13}\text{C}'\text{-Phe}_{12}^{19}\text{F}$  distances for the parallel dimer, 13.9 and 7.3 Å, are too short compared to the experimental data. An examination of the PG-1 solution structure indicates that the  $\phi$  angle of Cys<sub>13</sub>, around  $-90^\circ$ , deviates the most from the canonical  $\beta$ -sheet  $\phi$  angle. Thus, we modified the  $\phi$  angle of the same residue in the ideal  $\beta$ -strand model. With  $\phi_{13} = -65^\circ$ , we obtained intermolecular  $\text{C}'\text{-F}$  distances of 15 and 10 Å, which agree roughly

with the experimental data (Figure 4d). In contrast, the distances in the antiparallel dimer of this nearly ideal  $\beta$ -strand are too short ( $\sim 6$  Å) to satisfy the experimental data. Thus, the parallel packing result does not require the membrane-bound PG-1 to have the same  $\phi$ ,  $\psi$  angles as in solution. The C-strand of PG-1 could adopt a more ideal, although not perfect,  $\beta$ -sheet structure in the bilayer, and the same parallel packing conclusion still holds.

**$^1\text{H}\{^{13}\text{C}\}$  REDOR.** To further constrain the dimer interface structure, we measured the  $^1\text{H}^{\text{N}}-^{13}\text{C}'$  dipolar coupling between Cys<sub>15</sub> residues in the equimolar mixture of PG-1. As seen above, the  $^{15}\text{N}-^{13}\text{C}$  dipolar coupling between the same two labeled sites is too weak to serve as useful distance constraints. This is remedied in the  $^1\text{H}\{^{13}\text{C}\}$  REDOR experiment because  $^1\text{H}$  spins have a 10-fold larger gyromagnetic ratio than  $^{15}\text{N}$ , increasing the dipolar coupling strength. The  $^1\text{H}\{^{13}\text{C}\}$  REDOR experiment is based on the principle that only a single proton, the amide proton directly bonded to the labeled  $^{15}\text{N}$ , is measured in terms of its dipolar coupling to the labeled  $^{13}\text{C}'$ . This selective REDOR dephasing is achieved by the use of a short (75  $\mu\text{s}$ ) and spin diffusion-free  $^1\text{H}-^{15}\text{N}$  LG-CP, which transfers only the  $\text{H}^{\text{N}}$  magnetization to  $^{15}\text{N}$  for detection, and by homonuclear  $^1\text{H}$  decoupling during the REDOR mixing time (16, 26).

Figure 6a shows representative  $^{15}\text{N}$ -detected  $^1\text{H}\{^{13}\text{C}\}$  REDOR spectra of the mixed PG-1 sample and the  $S/S_0$  values. The dephasing due to natural abundance  $^{13}\text{C}$  sites had been corrected by an independent experiment on a  $^{15}\text{N}$ -Cys<sub>15</sub>-labeled PG-1 sample. The  $S/S_0$  values reach a plateau of 0.73 at 2.3 ms. The minimum  $S/S_0$  value attainable by a fully dimerized and 1:1 statistically mixed labeled peptide is 0.50. If the dimer fraction is 88%, then the minimum possible REDOR intensity would be  $1 - 0.88/2 = 0.56$ . Since the measured minimum REDOR intensity is 0.73, much higher than these two values, the system must contain both a short and a long distance so that the weak coupling due to the long distance does not contribute significantly to dephasing. This short and long distance motif (Figure 6b) is consistent with the parallel dimer structure determined from the  $^{13}\text{C}\{^{19}\text{F}\}$  REDOR experiment. The best fit to the C-H REDOR data is obtained using a short distance of  $2.5 \pm 0.2$  Å and a long distance of  $6.5 \pm 0.5$  Å (Figure 6a). The dephasing is primarily sensitive to the strong coupling: calculated curves using 2.3 Å (dotted line) and 2.7 Å (dashed line) for the short distance and the same long distance of 6.5 Å deviate noticeably from the experimental data (Figure 6a).

The C-H REDOR data constrain the percentage of dimerization at the P/L of 1:20. Our previous CODEX experiments showed that the dimer fraction is 60% at a P/L of 1:35 and 88% at a P/L = 1:12.5 (9). These suggest an intermediate dimer fraction of  $\sim 75\%$  at P/L = 1:20. However, the calculated REDOR intensities for this reduced dimer fraction are too high compared to the experimental intensities at long mixing times. In fact, the minimum REDOR intensity for a 100% dimerized parallel dimer is  $\sim 0.73$ , due to the 1:1 statistical mixing and the combination of a strong and a weak coupling in the parallel dimer structure. Since the experimental  $S/S_0$  value at 2.3 ms is  $0.73 \pm 0.08$ , the dimer fraction must be close to the 90% measured previously on the 1:12.5 sample (9). The similarity of the dimer fraction at 1:20 and 1:12.5 P/L ratios suggests that

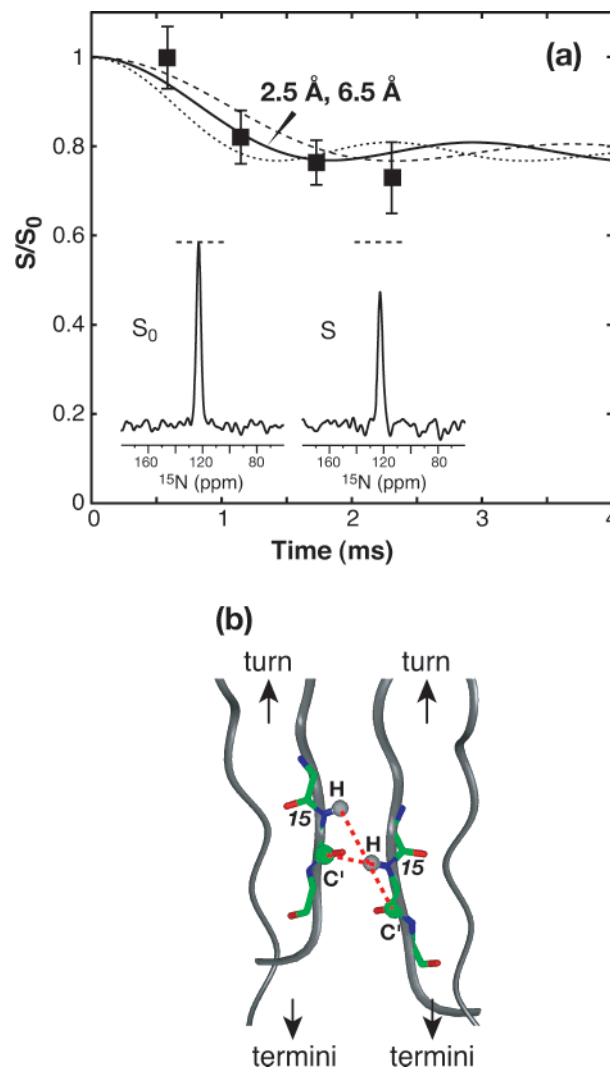


FIGURE 6: (a)  $^{15}\text{N}$ -Detected  $^1\text{H}\{^{13}\text{C}\}$  REDOR spectra of the 1:1 mixture of [ $^{13}\text{C}'$ -Cys<sub>15</sub>]PG-1 and [ $^{15}\text{N}$ -Cys<sub>15</sub>]PG-1 in POPC bilayers (P/L = 1:20) at a mixing time of 1.73 ms. The natural-abundance corrected  $S/S_0$  values are best fit (solid line) to distances of 2.5 and 6.5 Å. To show the uncertainty of the shorter distance, the REDOR simulations for 2.7 and 6.5 Å (dashed line) and for 2.3 and 6.5 Å (dotted line) are also shown. A dimer fraction of 88% is used in all simulations. (b) Illustration of the intermolecular  $^{13}\text{C}'-^1\text{H}^{\text{N}}$  Cys<sub>15</sub> distances (red dashed lines) in the NCCN parallel dimer.

dimerization is a cooperative process: once the peptide concentration reaches a threshold, dimerization is nearly complete. This cooperativity of structural transition has been experimentally observed in several antimicrobial peptides, including PG-1, by X-ray and neutron scattering and by oriented circular dichroism experiments (27, 28). Oligomerization cooperativity is also common in other membrane peptides such as the M2 peptide of influenza A virus (29).

**Registry of Intermolecular Hydrogen Bonds.** The two NCCN dimer models we considered so far assume that the C-strands are aligned in register, so that six hydrogen bonds, the maximum possible, are established. We designate this in-register hydrogen-bonding motif as  $(i, j)$ . To assess whether this in-register structure uniquely agrees with the experimental data, we considered the intermolecular distances in out-of-register packing models. The most likely out-of-register hydrogen-bonding motifs are  $(i, j - 2)$  and  $(i, j + 4)$  for parallel packing and  $(i, j + 2)$  and  $(i, j - 2)$  for

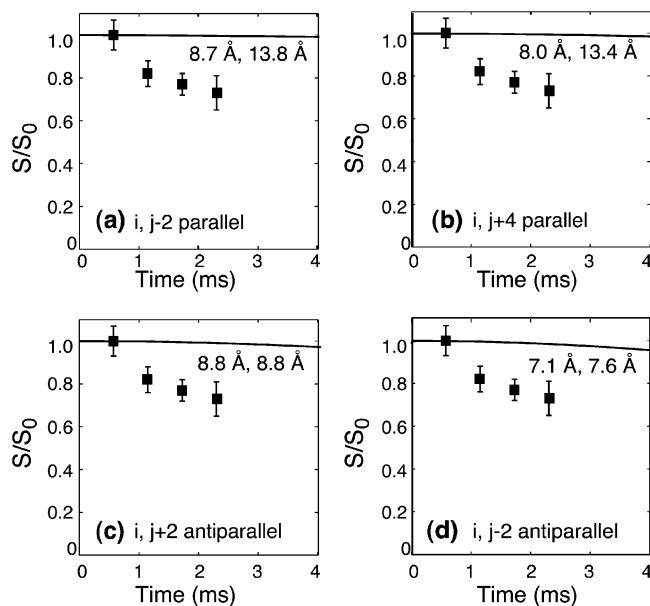


FIGURE 7: Simulated  $\text{H}^{\text{N}}-\text{C}'$  REDOR curves for out-of-register NCCN hydrogen-bonding motifs. (a)  $(i, j - 2)$  parallel packing. (b)  $(i, j + 4)$  parallel packing. (c)  $(i, j + 2)$  antiparallel packing. (d)  $(i, j - 2)$  antiparallel packing. None of these out-of-register packing models agree with the experimental data.

antiparallel packing. These were obtained by shifting one C-strand relative to the other by an even number of residues. The  $(i, j + 2)$  parallel dimer is isomorphous with the original  $(i, j)$  parallel dimer and thus is not considered. Only even-number shifts are possible because every other residue on the C-strand forms intramolecular hydrogen bonds with the N-terminal strand of the same molecule. On the basis of these models, we calculated the intermolecular  $^1\text{H}^{\text{N}}-^{13}\text{C}'$  REDOR curves between  $\text{Cys}_{15}$  (Figure 7). None of the out-of-register packing motifs agree with the experimental  $\text{H}^{\text{N}}-\text{C}'$  REDOR data. The shift in registry lengthens the distance significantly so that the REDOR dephasing is minimal compared to the experimental data. Thus, the in-register parallel packing with six intermolecular hydrogen bonds is the only structure consistent with the REDOR data.

Figure 8 shows the PG-1 NCCN parallel dimer structure that agrees with all REDOR distance constraints measured here. The measured REDOR distances are shown as red dotted lines. The intermolecular hydrogen bonds, formed between the odd-numbered residues, are shown as black dashed lines. Near the end of the C-strand, the putative hydrogen bonds are longer due to the disorder in the solution structure. In the lipid membrane, these terminal hydrogen bond lengths should shorten since the lipid bilayer is likely to induce a more ideal  $\beta$ -strand conformation (30).

## DISCUSSION

While a number of  $\alpha$ -helical membrane peptides such as K3, glycoporphin A, and PGLa have been shown or postulated to dimerize in the membrane (6, 31–33), few studies of  $\beta$ -sheet peptide aggregation in the lipid bilayer have been reported (34). The current study is the first time the oligomeric structure of a  $\beta$ -hairpin peptide is directly determined in the lipid bilayer. On the basis of the dimer stoichiometry found in POPC bilayers from our previous  $^{19}\text{F}$  spin diffusion experiment, we analyzed the REDOR curves

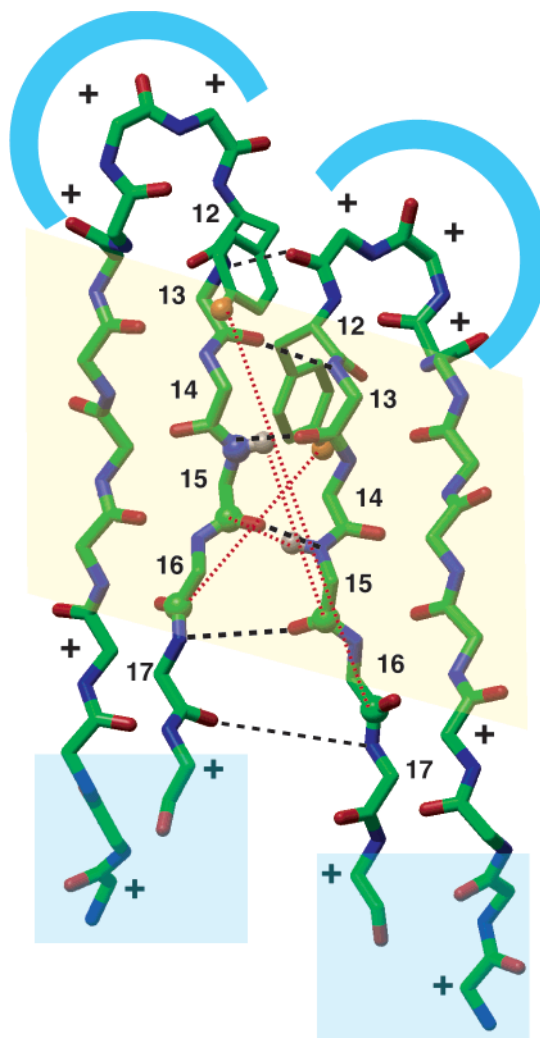


FIGURE 8: Structure of the NCCN parallel dimer of PG-1 in POPC bilayers. The measured REDOR distances are shown as red dotted lines. Intermolecular hydrogen bonds  $\text{R}_{\text{N}-\text{O}}$  are indicated as black dashed lines. The charged Arg residues are indicated by the (+) signs. The hydrophilic and hydrophobic regions of the peptide dimer are highlighted by blue and orange shaded areas, respectively, to emphasize the amphipathic character of the dimer.

for three heteronuclear couplings,  $^{13}\text{C}-^{19}\text{F}$ ,  $^1\text{H}-^{13}\text{C}$ , and  $^{13}\text{C}-^{15}\text{N}$  between C-strand labeled residues. The fact that all three couplings give measurable REDOR decays indicates that the C-strand of the peptide forms the oligomeric interface in an NCCN fashion. The long  $^{13}\text{C}'-^{19}\text{F}$  distances measured between the covalently well separated  $\text{Val}_{16}$  and  $\text{Phe}_{12}$  indicate that the two  $\beta$ -hairpins are aligned in a parallel fashion. The intermolecular  $^1\text{H}^{\text{N}}-^{13}\text{C}'$  distances between  $\text{Cys}_{15}$  residues further restrains the dimer interface structure, eliminating out-of-register packing motifs that have fewer than six intermolecular hydrogen bonds.

Is a mixture of dimer packing motifs compatible with the experimental data? For example, can both NCCN and CNNC dimers coexist in the sample? The  $^1\text{H}-^{13}\text{C}$  and  $^{15}\text{N}-^{13}\text{C}$  REDOR data on the  $\text{Cys}_{15}$ -labeled peptides exclude this possibility. If CNNC dimers are present at a significant percentage, then its corresponding  $\text{Cys}_{15}-\text{Cys}_{15}$  distances would be in the  $\sim 14$  Å range. This would produce no dephasing on the experimentally accessible  $^1\text{H}-^{13}\text{C}$  or the  $^{15}\text{N}-^{13}\text{C}$  REDOR time scales. Similarly, the shortest  $\text{H}^{\text{N}}-\text{C}'$  distance physically possible between two  $\text{Cys}_{15}$  residues

cannot be much shorter than the experimentally measured value of  $2.5 \pm 0.2$  Å. Thus, it is not possible to fit the experimental  $^1\text{H}\{^{13}\text{C}\}$  REDOR data by a combination of long distances from the CNNC or NCNC dimer motifs and short distances from the NCCN model. This rules out any significant presence of CNNC or NCNC dimers where the C-strand labels are far away from each other.

On the other hand, the current REDOR data do not rule out the presence of higher order oligomers of the type ...NCCNCCN... where every C-strand oligomerizes with another C-strand and every N-strand interfaces with another N-strand, since no N-strand labels are used to measure distances between N-strands. While the previous  $^{19}\text{F}$  spin diffusion experiment detected only a dimer, the technique has a distance upper limit of  $\sim 15$  Å. From the  $^{19}\text{F}$ -labeled Phe<sub>12</sub> on the C-strand, it would not be possible to detect, beyond the immediate C-strand interface, another  $^{19}\text{F}$  spin in the next C-strand interface if it were more than 15 Å away. Thus, an extended like-strand packing motif  $(\text{NCCN})_n$  can be compatible with the current REDOR data. Outside the membrane, we found that PG-1 can be induced to form ordered "fibrils" with a tight C-strand interface and a loose N-strand interface (35). Thus, an oligomer of NCCN dimers is conceivable in the POPC membrane. However, this possibility does not change the conclusions about the C-strand interface structure obtained from the REDOR data here.

The homo-oligomerization of two C-strands is favored by the strong hydrophobic nature of the C-strand due to its scarcity of Arg (Figure 2). The C-strand residues also have relatively short side chains, thus facilitating close packing of the two monomers (36). The parallel alignment of the hairpins is noteworthy. A solution NMR study of PG-1 in DPC micelles (37) found that the peptide forms antiparallel NCCN dimers, in contrast to our result in lipid bilayers, although no information is available on how the antiparallel PG-1 dimer is incorporated into the micelle. The different alignment likely results from the significant curvature difference between the small-radius micelles and the flatter and more biological lipid bilayers. In the lipid bilayer, an important driving force for parallel packing of PG-1 may be the formation of a continuous Arg surface at the  $\beta$ -turns. A total of six Arg residues would cluster in a small region in the parallel dimer, separated from the N- and C-terminal Arg residues by a region of ten hydrophobic residues (Figure 8). Thus, the parallel dimer has a strong amphipathic character. The cationic Arg surface at the  $\beta$ -turn should have very favorable electrostatic interactions with the anionic phosphate of the lipid headgroup. The amphipathic dimer may also insert into the membrane more readily. The crystal structure of  $\alpha$ -defensin HNP-3, an antimicrobial peptide containing a  $\beta$ -sheet domain, shows an antiparallel dimer of the  $\beta$ -sheet (38) that results in a strong hydrophilic–hydrophobic separation. This led to the hypothesis that this amphipathic dimer may insert into the lipid bilayer like a wedge, with the nonpolar side facing the lipid acyl chains. The PG-1 parallel dimer, which has a similarly strong amphipathic character, may also insert into the lipid membrane more readily than a monomer. The different packing motifs of PG-1 between the lipid bilayer and the micelle underscore the importance of the environment for the oligomerization

of membrane peptides and the plasticity of the PG-1 structure.

The PG-1 parallel dimer has an overall length of  $\sim 30$  Å. Our previous  $^1\text{H}$  spin diffusion measurements showed that the peptide is well inserted into the hydrophobic part of the POPC membrane (39), which has a P–P distance of  $\sim 45$  Å. However, the POPC bilayer in the presence of the peptide shows significant structure distortion, as manifested by the  $^{31}\text{P}$  spectra (13). This suggests that, instead of the normal lamellar structure of liquid-crystalline bilayers, the peptide-bound POPC membrane contains a significant number of defects, such as toroidal pores, at the location of these PG-1 dimers. How the peptide–membrane hydrophobic mismatch is resolved at the defect sites will be interesting for further study.

The PG-1 dimer structure reported here is determined in zwitterionic POPC bilayers. This model membrane oligomeric structure establishes a necessary baseline to which future structural studies in more biologically relevant membrane compositions can be compared. Such membranes include bacteria-mimetic anionic lipid bilayers as well as cholesterol-rich neutral bilayers that mimic red blood cell membranes.

## REFERENCES

- Reddy, K. V., Yedery, R. D., and Aranha, C. (2004) Antimicrobial peptides: premises and promises, *Int. J. Antimicrob. Agents* 24, 536–547.
- Hancock, R. E., and Lehrer, R. (1998) Cationic peptides: a new source of antibiotics, *Trends Biotechnol.* 16, 82–88.
- Bechinger, B. (1999) The structure, dynamics, and orientation of antimicrobial peptides in membranes by multidimensional solid-state NMR spectroscopy, *Biochim. Biophys. Acta* 1462, 157–183.
- Strandberg, E., and Ulrich, A. S. (2004) NMR methods for studying membrane-active antimicrobial peptides, *Concepts Magn. Reson.* 23, 89–120.
- Epanand, R. M., and Vogel, H. J. (1999) Diversity of antimicrobial peptides and their mechanisms of action, *Biochim. Biophys. Acta* 1462, 11–28.
- Toke, O., O'Connor, R. D., Weldeghiorghis, T. K., Maloy, W. L., Glaser, R. W., Ulrich, A. S., and Schaefer, J. (2004) Structure of  $(\text{KIAGKIA})_3$  aggregates in phospholipid bilayers by solid-state NMR, *Bioophys. J.* 87, 675–687.
- Kokryakov, V. N., Harwig, S. S., Panyutich, E. A., Shevchenko, A. A., Aleshina, G. M., Shamova, O. V., Korneva, H. A., and Lehrer, R. I. (1993) Protegrins: leukocyte antimicrobial peptides that combine features of corticostatic defensins and tachyplesins, *FEBS Lett.* 327, 231–236.
- Bellm, L., Lehrer, R. I., and Ganz, T. (2000) Protegrins: new antibiotics of mammalian origin, *Expert Opin. Invest. Drugs* 9, 1731–1742.
- Buffly, J. J., Waring, A. J., and Hong, M. (2005) Determination of peptide oligomerization in lipid membranes with magic-angle spinning spin diffusion NMR, *J. Am. Chem. Soc.* 127, 4477–4483.
- Searle, M. S., and Ciani, B. (2004) Design of  $\beta$ -sheet systems for understanding the thermodynamics and kinetics of protein folding, *Curr. Opin. Struct. Biol.* 14, 458–464.
- Wimley, W. C. (2003) The versatile  $\beta$ -barrel membrane protein, *Curr. Opin. Struct. Biol.* 13, 404–411.
- Gullion, T., and Schaefer, J. (1989) Rotational echo double resonance NMR, *J. Magn. Reson.* 81, 196–200.
- Yamaguchi, S., Hong, T., Waring, A., Lehrer, R. I., and Hong, M. (2002) Solid-state NMR investigations of peptide-lipid interaction and orientation of a  $\beta$ -sheet antimicrobial peptide, protegrin, *Biochemistry* 41, 9852–9862.
- Sinha, N., Schmidt-Rohr, K., and Hong, M. (2004) Compensation for pulse imperfections in rotational-echo double-resonance NMR by composite pulses and EXORCYCLE, *J. Magn. Reson.* 168, 358–365.

15. Gullion, T., Baker, D. B., and Conradi, M. S. (1990) New, compensated Carr-Purcell sequences, *J. Magn. Reson.* **89**, 479–484.
16. Schmidt-Rohr, K., and Hong, M. (2003) Measurements of carbon to amide-proton distances by C-H dipolar recoupling with  $^{15}\text{N}$  NMR detection, *J. Am. Chem. Soc.* **125**, 5648–5649.
17. Wi, S., Sinha, N., and Hong, M. (2004) Long range  $^1\text{H}$ - $^{19}\text{F}$  distance measurement in peptides by solid-state NMR, *J. Am. Chem. Soc.* **126**, 12754–12755.
18. Mansfield, P. (1971) Symmetrized pulse sequences in high-resolution NMR in solids, *J. Phys. C: Solid State Phys.* **4**, 1444.
19. Rhim, W.-K., Elleman, D. D., and Vaughan, R. W. (1973) Analysis of multiple-pulse NMR in solids, *J. Chem. Phys.* **59**, 3740–3749.
20. Bak, M., Rasmussen, T., and Nielsen, N. C. (2000) SIMPSON: A general simulation program for solid-state NMR spectroscopy, *J. Magn. Reson.* **147**, 296–330.
21. Bak, M., and Nielsen, N. C. (1997) REPULSION, a novel approach to efficient powder averaging in solid-state NMR, *J. Magn. Reson.* **125**, 132–139.
22. Fahrner, R. L., Dieckmann, T., Harwig, S. S., Lehrer, R. I., Eisenberg, D., and Feigon, J. (1996) Solution structure of protegrin-1, a broad-spectrum antimicrobial peptide from porcine leukocytes, *Chem. Biol.* **3**, 543–550.
23. Sali, A., and Blundell, T. L. (1993) Comparative protein modeling by satisfaction of spatial restraints, *J. Mol. Biol.* **234**, 779–815.
24. deDios, A. C., and Oldfield, E. (1994) Chemical shifts of carbonyl carbons in peptides and proteins, *J. Am. Chem. Soc.* **116**, 11485–11488.
25. Lovell, S. C., Word, J. M., Richardson, J. S., and Richardson, D. C. (2000) The penultimate rotamer library, *Proteins: Struct., Funct., Genet.* **40**.
26. Sinha, N., and Hong, M. (2003) X- $^1\text{H}$  rotational-echo double-resonance NMR for torsion angle determination of peptides, *Chem. Phys. Lett.* **380**, 742–748.
27. Huang, H. W. (2006) Molecular mechanism of antimicrobial peptides: the origin of cooperativity, *Biochim. Biophys. Acta* (in press).
28. Huang, H. W. (2000) Action of antimicrobial peptides: two-state model, *Biochemistry* **39**, 8347–8352.
29. Stouffer, A. L., Nanda, V., Lear, J. D., and DeGrado, W. F. (2005) Sequence determinants of a transmembrane proton channel: an inverse relationship between stability and function, *J. Mol. Biol.* **347**, 169–179.
30. Wimley, W. C., Hristova, K., Ladokhin, A. S., Silverstro, L., Axelsen, P. H., and White, S. H. (1998) Folding of  $\beta$ -sheet membrane proteins: a hydrophobic hexapeptide model, *J. Mol. Biol.* **277**, 1091–1110.
31. Smith, S. O., Song, D., Shekar, S., Groesbeek, M., Ziliox, M., and Aimoto, S. (2001) Structure of the transmembrane dimer interface of glycophorin A in membrane bilayers, *Biochemistry* **40**, 6553–6558.
32. Glaser, R. W., Sachse, C., Durr, U. H., Wadhvani, P., Afonin, S., Strandberg, E., and Ulrich, A. S. (2005) Concentration-dependent realignment of the antimicrobial peptide PGLa in lipid membranes observed by solid-state  $^{19}\text{F}$  NMR, *Biophys. J.* **88**, 3392–3397.
33. Murphy, O. J., Kovacs, F. A., Sicard, E. L., and Thompson, L. K. (2001) Site-directed solid-state NMR measurement of a ligand-induced conformational change in the serine bacterial chemoreceptor, *Biochemistry* **40**, 1358–1366.
34. Yang, J., and Weliky, D. P. (2003) Solid-state nuclear magnetic resonance evidence for parallel and antiparallel strand arrangements in the membrane-associated HIV-1 fusion peptide, *Biochemistry* **42**, 11879–11890.
35. Tang, M., Waring, A. J., and Hong, M. (2005) Intermolecular and alignment of a  $\beta$ -hairpin peptide fibril from 2D solid-state NMR, *J. Am. Chem. Soc.* **127**, 13919–13927.
36. Smith, S. O., Eilers, M., Song, D., Crocker, E., Ying, W., Groesbeek, M., Metz, G., Ziliox, M., and Aimoto, S. (2002) Implications of threonine hydrogen bonding in the glycophorin A transmembrane helix dimer, *Biophys. J.* **82**, 2476–2486.
37. Roumestand, C., Louis, V., Aumelas, A., Grassy, G., Calas, B., and Chavanieu, A. (1998) Oligomerization of protegrin-1 in the presence of DPC micelles. A proton high-resolution NMR study, *FEBS Lett.* **421**, 263–267.
38. Hill, C. P., Yee, J., Selsted, M. E., and Eisenberg, D. (1991) Crystal structure of defensin HNP-3, an amphiphilic dimer: mechanisms of membrane permeabilization, *Science* **251**, 1481–1485.
39. Buffy, J. J., Waring, A. J., Lehrer, R. I., and Hong, M. (2003) Immobilization and aggregation of the antimicrobial peptide protegrin-1 in lipid bilayers investigated by solid-state NMR, *Biochemistry* **42**, 13725–13734.
40. Bennett, A. E., Rienstra, C. M., Auger, M., Lakshmi, K. V., and Griffin, R. G. (1995) Heteronuclear decoupling in rotating solids, *J. Chem. Phys.* **103**, 6951–6958.
41. vanRossum, B. J., deGroot, C. P., Ladizhansky, V., Vega, S., and deGroot, H. J. M. (2000) A method for measuring heteronuclear ( $^1\text{H}$ - $^{13}\text{C}$ ) distances in high-speed MAS NMR, *J. Am. Chem. Soc.* **122**, 3465–3472.

BI060305B